Accepted Manuscript

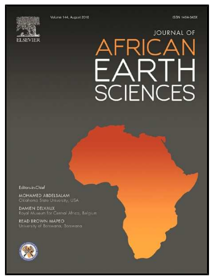

Distinguishing rift-related from inversion-related anticlines: Observations from the Abu Gharadig and Gindi Basins, Western Desert, Egypt.

Mohammad Abdelfattah Sarhan, Richard E. Ll. Collier

PII:	S1464-343X(18)30158-4
DOI:	10.1016/j.jafrearsci.2018.06.004
Reference:	AES 3230
To appear in:	*Journal of African Earth Sciences*
Received Date:	22 June 2017
Accepted Date:	05 June 2018

Please cite this article as: Mohammad Abdelfattah Sarhan, Richard E. Ll. Collier, Distinguishing rift-related from inversion-related anticlines: Observations from the Abu Gharadig and Gindi Basins, Western Desert, Egypt., *Journal of African Earth Sciences* (2018), doi: 10.1016/j.jafrearsci.2018.06.004

Distinguishing rift-related from inversion-related anticlines: Observations from the Abu Gharadig and Gindi Basins, Western Desert, Egypt.

Mohammad Abdelfattah Sarhan[1*] and Richard E. Ll. Collier[2]

[1]. Geology Department, Faculty of Science, Damietta University, Damietta, 34517, Egypt.
[2]. Basin Structure Group, School of Earth and Environment, University of Leeds, Leeds LS2 9JT, UK.
*msarhan@du.edu.eg

Abstract

Distinguishing the tectonic origin of anticlinal structures is problematic in regions with a complex history of rifting and inversion. We present the results of seismic mapping, in the form of time-depth (isochron) and time-thickness maps to characterize how sedimentary thickness differentials evolved in response to normal faulting and to inversion events on faults within the Abu Gharadig and Gindi Basins in the Western Desert of Egypt. Late Cretaceous rift-related faults in the Abu Gharadig Basin strike NW-SE, W-E and SW-NE. In the eastern part of the basin, a prominent SW-NE trending interbasinal saddle formed in response to preferential subsidence forming half-grabens to its north-west and southeast, during the Mid-Turonian to Santonian interval. Santonian to Palaeogene inversion in the Abu Gharadig Basin developed on its northern basin margin, the absence of SW-NE striking faults in the eastern central basin resulting in any inversion effects being minor. In the central Gindi Basin, Upper Cenomanian to Lower Turonian SW-NE striking rift faults underwent inversion as early as the Mid-Turonian. The orientation of existing rift faults and modification of the local stress fields control the extent to which inversion was taken up in each basin trough time. The Abu Gharadig and Gindi Basins are two of the rift basins developed in West and Central Africa that underwent rifting, inversion and dextral shearing during the Late Cretaceous. We emphasize the value of high-resolution stratigraphic mapping to characterize short-lived and subtle pop-up events that may have gone unnoticed.

Keywords: Anticlines - Rifting – Inversion tectonics - Abu Gharadig Basin - Gindi Basin.

1. Introduction

A common problem in the structural interpretation of rift basins with long and complex tectonic histories is the distinction of structural and stratigraphic geometries that are the product of extensional rifting from those that result from compression and structural inversion. A range of fold types may form in response to normal fault growth, either a) as a response to growing fault hanging wall and footwall displacement fields (e.g. Ellis and McClay, 1988; Schlische 1995; Contreras et al. 2000) or b) at a shorter wavelength, to the propagation of fault-tip monoclines (Wilson et al., 2009), or c) due to the interaction of displacement fields associated with adjacent normal faults (Morley et al., 1990; Cartwright et al., 1995; Dawers and Underhill 2000; Rotevatn and Jackson, 2014). Inversion of pre-existing normal faults and concurrent folding or tightening of rift-related folds may be a record of a change in the far-field stress regime from extension to compression (Cooper and Williams 1989; Coward 1991; Tavernelli 1996; Turner and Williams 2004; Scisciani 2009; Withjack et al., 2010; Bonini et al., 2012), or to the rotation of principal stress directions (e.g. Paton and Underhill 2004). The latter authors showed that subtle shifts in the orientation of the maximum deviatoric stress direction during rifting can create structures that in many cross-sections appear to be inversion features. There is a possibility that rift-related structures may be misinterpreted as due to structural inversion resulting from a switch to a regional compressive regime. Examples of inverted rift basins worldwide are many and include the Australian Dampier Sub-Basin (Cathro and Karner, 2006); the Cameros Basin in Spain (Salè et al., 2014) and the Brazilian Rio do Peixe Basin (Nogueira et al., 2015). Detection and interpretation of inversion features within rift basins, and their distinction from rift-related structures, is important for accurate deductions of orientations of principal stress axes and appreciation of the region's plate tectonic history through time.

Several hypotheses regarding the tectonic history of the Western Desert province in Egypt arose due to uncertainties in the origin and timing of anticlinal growth in various rift basins in the region. For example, Bayoumi and Lofty (1989) invoked a broad phase of Late Cretaceous to Early Cainozoic compression and inversion in the Western Desert. Whereas, Moustafa (2008) referred to continuous normal fault activity in the Late Cretaceous to Early Cainozoic along WNW-ESE striking faults, which are thought to be parallel to the contemporaneous shortening direction related to convergence of Afro-Arabia and Eurasia. Moustafa (2008) proposed that multiple pulses of inversion took place across the Western Desert in the Late Cretaceous to Oligocene, inverting early rift faults of NE-SW, ENE-WSW and NNE-SSW orientation and developing similarly oriented structural traps. Bosworth et al. (2008) noted that arc collisions on the north-east African margin from the Santonian onwards yielded varied structural expressions across the Western Desert, depending on whether the affected structure lay within the stress shadow of the Cyrenaican inversion belt. Shortening was most severe in a belt reaching from northern Libya across to the Levant and diminished to the south and east of this deformation belt. In this context, it is the northern margin of the Abu Gharadig Basin (Fig. 1) which has accommodated the major part of the shortening of this basin, across the Mubarak Inversion Complex (as illustrated in Bosworth et al. 2008). Moustafa (2013) proposed that the NE-SW orientation of the Abu Gharadig Field anticlinal trap was due to rift-related subsidence to both the NW and SE of the fold axis.

This study focuses on the Abu Gharadig and Gindi Basins in the Western Desert, Egypt (Figure 1), and illustrates the use of stratigraphic thickness changes in time-thickness maps as the primary tool to distinguish rift-related from inversion-related structural geometries. As outlined above, the different anticline geometries and orientations present across the adjacent basins have been explained by differing tectonic interpretations in the recent past. In this study, we aim to show that with detailed mapping, even where only a really restricted 2D seismic surveys are available, coherent tectonic interpretations can be derived from these data. We present time-depth maps of key stratigraphic surfaces within each basin, and then produce time-thickness maps for key intervals. These time thickness maps together with cross-sections are critical for distinguishing the timing of extensional activity on normal faults of varied orientations, and for isolating which fault orientations may have undergone any compressional inversion effects and when this occurred.

2. Geologic setting

The Triassic-Early Cretaceous rift basins in the northern Western Desert of Egypt resulted from the opening of the Tethys Ocean (e.g. Ziegler, 1987; Frizon de Lemotte et al., 2011) and subsequent inversion (Bayoumi and Lofty, 1989; Guiraud, 1998; Bosworth, 1994; Bosworth et al., 2008; Wescott et al., 2011). The Abu Gharadig Basin and the Gindi Basin are productive hydrocarbon basins in the northern part of the Egyptian Western Desert. Both basins originated as N- and NE-tilted half-grabens in the Jurassic-Early Cretaceous concurrent with the opening of the Neo-Tethys and Atlantic oceans (Moustafa, 2008).

The stratigraphy of the northern Western Desert, including both the Abu Gharadig and Gindi Basins is summarized in Figure 2. This study is focused on the Upper Cretaceous to Oligocene strata. The Late Cretaceous rock units are divided into three formations from base to top, the Bahariya, Abu Roash and Khoman Formations. The Bahariya Formation (Cenomanian age) conformably overlies the Early Cretaceous Kharita Formation (EGPC, 1992). It consists of fine to medium-grained sandstone with thin shale and carbonate interbeds (Soliman and El Badry, 1980; Schlumberger, 1984). The Bahariya Formation is thought to have been deposited by fluvial systems passing into inner shelf, shallow marine environments (Abd El Kireem et al., 1996).

The Abu Roash Formation (Turonian-Coniacian age) conformably overlies the Bahariya Formation and unconformably underlies the Khoman Formation. It is composed of alternations of carbonate and clastic rocks and is subdivided into seven members named A to G from top to base. It was deposited under shallow marine shelf conditions (Schlumberger, 1984; EGPC, 1992; Abd El Kireem et al., 1996) as successive oscillating transgressive-regressive marine cycles (Sarhan, 2017a). The Khoman Formation (Santonian-Maastrichtian age) overlies the Abu Roash Formation unconformably (Hantar, 1990; Abd El Kireem and Ibrahim, 1987; Schrank and Ibrahim, 1995) and comprises a thick chalky limestone section deposited under outer shelf conditions (Sultan and Halim, 1988; EGPC, 1992; Abd El Kireem et al. 1996; Tantawy et al., 2001; Mahsoub et al., 2012) during widespread sea-level rise covered most of the northern parts of Egyptian lands associated with basin subsidence (Sarhan, 2017a). It is subdivided into two members by an unconformity surface; the lower member B is composed of shale and argillaceous limestone whilst the upper A member is composed of chalky limestone (Fawzy and Dahi, 1992). These unconformities tend not to be obvious within depocentres, where continuous sedimentation resulted in their correlative conformities.

At the end of Cretaceous time, a marked depositional gap and erosional truncations developed over much of the Western Desert, during the Palaeocene (Schlumberger, 1984; EGPC, 1992). The Eocene Apollonia Formation unconformably overlies the Late Cretaceous Khoman Formation and consists of hard limestone and rare chalky limestones, with some shale intercalations deposited in an open marine environment (Fawzy and Dahi, 1992; EGPC, 1992; Bakry, 1993). The Oligocene Dabaa Formation is composed of a thick shale succession and overlies the Apollonia Formation unconformably (Fawzy and Dahi, 1992). It was deposited under inner-shelf to littoral environments, shallower than the depositional environment of the underlying Apolonia Formation (EGPC, 1992).

Most of the hydrocarbons in the Western Desert, including in the Abu Gharadig and Gindi Basins were discovered by targeting structural prospects in sandstone and carbonate reservoirs (e.g. Sarhan et al., 2017a & b). These structural traps appear as three-way fault-bounded or elongate, dome-like four-way closures, within the Cretaceous sedimentary package (e.g. Sarhan, 2017b; Sarhan et al., 2017b). These traps formed when Upper Cretaceous tectonic inversion affected the northern part of the Western Desert (Sultan and Abd El Halim 1988; EGPC, 1992, and David et al., 2003). Structural geometries in the inverted basins display great variation from one basin to another, depending on the pre-inversion structure of each basin.

The present work aims to characterize the orientation of inversion structures in the Abu Gharadig Basin and the Gindi Basin, to understand how Upper Cretaceous tectonic inversion affected the two sedimentary basins in the northern Western Desert of Egypt.

3. **Data and methodology**

The first study area is the central part of the Abu Gharadig Basin in the northern Western Desert that lies between latitudes 29.5^{o} and 30^{o} N and between longitudes 28.3^{o} and 28.8^{o} E (Figure 1). The seismic data available for this study were 30 (thirty) 2D migrated seismic reflection profiles at 2 km spacing extracted from a 3D seismic cube. Eleven (11) seismic lines-oriented ENE-WSW are up to 55.5 km long, and nineteen lines are oriented NNW-SSE trend and 25.5 km (Figure 3a). These seismic sections are tied to five wells (AG-2, AG-5, AG-6, AG-15 and SAWAG-1).

The second study area lies between latitudes 29.7^{o} and 29.8^{o} N and longitudes 30.4^{o} and 30.5^{o} E within the central part of the Gindi Basin (Figure 1). The available data comprised 20 (twenty) 2D migrated seismic reflection sections, comprising eleven of N-S orientation and nine trending E-W (Figure 3b). These seismic data sets are tied to three wells, SWQ-4, SWQ-21 and SWQ-25.

The procedures used in the present work to achieve the aim of the paper are a) the picking of faults in each basin, and b) the picking of distinct and laterally extensive seismic horizons, which are tied to the stratigraphic data from the wells in the basins. The interpreted faults and key horizons were mapped over the grid of 2D seismic lines to construct time-depth (isochron) maps, which allow the preparation of time-thickness (time-isochore) maps for each stratigraphic interval.

4. Results

4.1. Abu Gharadig Basin

Within this dataset, five seismic reflectors represent the clearest surfaces along all the examined seismic profiles. These surfaces display strong, relatively continuous and high amplitude reflectors across the seismic profiles (Figures 4a and b). According to the well-seismic ties, these horizons represent: (a) the top of the Bahariya Formation (green), varying in time-depth from 1400 to 2900 ms (Figure 2); (b) the top of the Abu Roash D Member (pale blue) that ranges from 1300 to 2500 ms in time-depth; (c) a high amplitude reflector designated near the top of Khoman B Member (yellow), picked higher than the real top of Khoman B surface by about 50 ms and varying in time-depth between 800 and 1800 ms; (d) near the top of Khoman A Member (pink), picked about 150 ms higher than the real top of Khoman A surface, ranging in time-depth from 500 to1300 ms; and (e) the uppermost horizon being a near-top Dabaa Formation surface (dark blue) at about 100 ms below the true top Dabaa Formation, and which varies in time-depth between 300 and 625 ms.

Fault picks reveal that all the interpreted faults in this study area have net normal (extensional) offsets. The time-depth maps for the interpreted surfaces show that the faults form two groups, faults of NW-SE trend with lengths between 5 km and at least 16 km, and faults of approximately E-W trend, which range in length from 5km to at least 20 km (Figure 5). These intrabasinal fault trends compare with the Abu Gharadig Basin border faults, which have NE-SW to E-W to ESE-WNW strikes (Figure 1). Note that the map areas presented in Figure 5 and other figures have been trimmed to avoid edge effects in the contouring.

The largest fault in this area forms one of the Abu Gharadig basin-bounding faults with throw ranging from 900 ms up to about 1100 ms at top-Bahariya level (F1, coloured red in Figure 4b and in Figure 5). Sedimentary strata in the hanging wall of this main fault have a component of dip toward its plane and form a significant dip-fan into the fault across all Upper Cretaceous to Oligocene mapped intervals, suggesting persistent reactivation and progressive rotation of the fault block during basin infilling episodes on its hanging wall side.

Mapped surfaces (Figure 5) are tilted to the north and north-west, towards the basin-bounding fault set that lies outside this study area, but which controls the northern margin of the Abu Gharadig Basin (Figure 1). The northern basin margin is delimited by E-W trending faults (Bosworth et al., 2008). An anticline in the central part of the study area trends NE-SW and includes the structural closure of the Abu Gharadig Field (Moustafa, 2008). This anticline is prominent at Top Bahariya and Top Abu Roash D levels (Figures 5a and 5b).

Line 5240 (Figure 4b) shows a major E-W fault (F2, coloured green) which downthrows to the north with significant offsets at Top Bahariya Formation and Top Abu Roash D levels. In other lines, it is clear that this fault cuts through all the interpreted horizons from the Top Bahariya horizon up to the Near-top Dabaa Formation horizon (Figure 5). Growth on this fault (and associated secondary faults of similar orientation) during the Top Abu Roash D Member to near the top of Khoman B Member interval contributed to the formation of the anticlinal closure, as did growth in the hanging wall to the F1 fault of opposite dip. The anticline may be considered to lie in the hanging wall of F1, the more major fault of the two, because all picked stratigraphic surfaces of the anticline are at a lower structural level than the equivalent surfaces in the footwall to F1, as seen in the WSW-ENE oriented line of section in Figure 4b.

The time-thickness maps for the four intervals bounded by the five interpreted horizons are presented in Figure 6. The Top Bahariya Formation to Top Abu Roash D interval (Figure 6a) displays thickening over the area of study to the north-west, into the northern basin margin fault set, and thickening to the north-east into the F1 NW-SE trending normal fault. Extension was thus being taken up on these faults and secondary faults of E-W to NW-SE strike during this period.

The second time-thickness map displays the interval between Top Abu Roash D and near the top of Khoman B Member (Fig. 6b) and shows a significant thickening to the NE again, towards fault F1 of NW-SE strike, with time-thickness values reaching 750 ms on the downthrown side of the fault. Also prominent within this time interval is thickening on either side of the Abu Gharadig central antiform. Within our study area, thicknesses can be seen to increase northwestwards to the north-west of this structure and to increase to the east southeast to the southeast of this antiform. Faults active within the study area are oriented E-

W to NW-SE, but the thickening to the NW and ESE of the antiform implies that faults at the basin margins to the north (dipping S or SE) and to the south-east (dipping NW) were controlling sedimentary thickening, such that the antiform formed as a saddle between two half-grabens of opposing dip during this period of active rifting. This saddle thus formed an interbasinal high between two fault-controlled depocentres of opposing polarity.

The time-thickness map of the stratigraphic interval between the near the top of Khoman B and near the top of Khoman A surfaces (Fig. 6c) displays less dramatic thickness differentials of up to 200 ms TWT in the study area. This suggests either less variable sedimentation rates with lesser tectonic activity during this period of deposition or a period of basin under filling. In the south and east of the study area, thicknesses increase toward the basin margin that lay to the southeast. In the north of the study area, thicknesses increase on the south-west, downthrown side of F1, indicating continued normal displacement on this structure. Thicknesses also increase to the north-west of the central antiform axis. Within the limited area mapped in this study, it is not clear whether the thickness differentials toward the northern and southeastern basin margins were due to continued extensional growth on basin margin faults or due to thickening into inversion-related growth synclines to NW and SE. The marker horizons remain below their regional levels, in net extension. Either way, the central antiform saddle is accentuated by differential subsidence to the north or north-west and to the south of its axis during this interval.

The time-thickness map of Figure 6d represents the interval from near the top of Khoman A to near the top of Dabaa Formation, which post-dates the Cretaceous-Palaeogene unconformity. This interval again shows a significant increase in thickness on the downthrown side of the F1 NW-SE trending normal fault. However, across the study area, thicknesses increase toward the NNW to a maximum time-thickness of 680 ms and higher values toward the northern basin margin faults. There is no expression of the central high or saddle. The south-dipping half-graben to the south of the Abu Gharadig anticline was therefore inactive. Reactivation of rifting therefore appears to have been focused onto F1 and the northern basin margin during this episode, with only minor faulting on secondary faults within the study area. It is worth noting that compared to the frequency of syn-depositionally active NW-SE faults during the Top Abu Roash D to near the top of Khoman B interval (Figure 6b), in the southern part of the study area, the near the top of Khoman A to near the top of Dabaa Formation interval (Figure 6d) is characterised by activity across E-W to WNW-ESE faults in the study area, except for reactivation of F1.

4.2. El-Gindi Basin

Seismic horizons within the grid of 2D lines from the central Gindi Basin (Figures 1 and 3) have been picked corresponding to the Top Bahariya Formation (yellow in Figure 7), Top Abu Roash F Member (blue), Top Abu Roash D Member (dark green) and Top Abu Roash B Member (light green), as constrained by ties to the wells SWQ-4, SWQ-21 and SWQ-25.

All picked horizons on the seismic sections display a clear anticline bounded by two faults, which show modest net reverse fault offsets of about 10-100 ms TWT at all the picked stratigraphic levels (Figure 7a, b and c). There is, however, some along-strike variation with the fault to the southeast of the anticline retaining a net extensional offset (e.g. Figure 7c). The time-depth maps for the picked horizons reveal a distinctive anticline, the axis of which plunges toward the NE and which is bounded by the two, 4-5 km long, NE–SW striking reverse faults (Figure 8).

The first time-thickness map for the Top Bahariya to Top Abu Roash F interval (Figure 9a) displays thinning to the south-west and south of the mapped faults. The interval shows slight thickening within the area bounded by the two faults, in the northeast of the mapped area. This suggests that these faults were active normal faults during this episode, the upper Cenomanian to lower Turonian, and controlled the formation of a minor graben in the central Gindi Basin.

The second time-thickness map (Figure 9b), of the interval between Top Abu Roash F and Top Abu Roash D (middle Turonian), shows a clear thinning in the area between the two interpreted NE-SW faults and thickening to the north-west and south-east of these (see also Figure 7). This suggests that these faults were active in the middle Turonian time interval as reverse faults. The time-thickness differential is up to ca. 40 ms TWT, from 190 ms TWT within the faults to 230 ms TWT outside the faults.

The third time-thickness map (Figure 9c) represents the interval between the Top Abu Roash D Member and the Top Abu Roash B Member (middle to upper Turonian). There is subtle thinning in the area between the two interpreted NE-SW faults and thickening to the north-west and southeast of the faults. This suggests that the faults continued to behave as reverse faults into the middle to upper Turonian, although with a thickness differential of only ca. 10 ms TWT.

5. Discussion and Conclusions

In many petroleum provinces, positive basin inversion structures represent important structural hydrocarbons traps (e.g. Bally, 1983; Fraser and Gawthorpe, 1990). The timing of hydrocarbon migration relative to the development of inversion structures is also critical in establishing a viable petroleum play, i.e. whether the migration may have occurred before or during or after the tectonic inversion (Sibson, 1995). In this study, we have constrained the structural timing element regarding Late Cretaceous rifting and tectonic inversion events in hydrocarbon-bearing sedimentary basins in the northern Western Desert, in the Abu Gharadig and Gindi Basins.

In lower Turonian times, both the Abu Gharadig Basin and the Gindi Basin show evidence of extensional faulting on faults with strikes ranging from NE-SW to E-W to NW-SE, implying a maximum deviatoric stress (extension) direction of approximately N-S. Through the mid-Turonian to Santonian history of the eastern Abu Gharadig Basin, a prominent saddle developed as a high between two opposing half-graben depocentres that were controlled by basin margin faults. This forms the prominent NE-SW striking faulted antiform of the Abu Gharadig Field (Moustafa, 2008). In contrast, detailed mapping has shown that after Cenomanian-lower Turonian rift faulting a subtle inversion event took place in the central Gindi Basin during the mid-Turonian, continuing into the upper Turonian. This was accommodated by the reverse offset of NE-SW striking faults. This event may be an early expression of the dextral shear environment across the West and Central African rift system and the rifts of the Western Desert and Sudan that existed throughout the Santonian to Maastrichtian (Fairhead et al., 2013). Pulses of rifting and inversion occurred as responses to changes in the intraplate stress regime that were driven by changes in spreading rates and azimuthal directions in the Central and South Atlantic oceans. In this context, minor mid-Turonian inversion of NE-SW faults in the Gindi Basin could be considered as a “pop-up” in a local dextral shear phase, with NE-SW maximum extension and NW-SE compression directions. The clear absence of this mid-Turonian inversion in the nearby Abu Gharadig Basin could be explained as due to either a) it not being resolved seismically and stratigraphically, or b) the absence of NE-SW striking faults within the mapped area, i.e.

faults of an orientation suitable for pop-up development, or c) the local stress field in the Abu Gharadig Basin not having a significant deviatoric compressional component.

The Top Abu Roash D Member to near the top of Khoman B interval, mid-Turonian to Santonian, in the Abu Gharadig Basin shows net extensional displacements on faults within the basin and on the NW-SE oriented basin margin fault (F1 in Figure 4b). This does not contradict the initiation of inversion on the northern margin of the basin during the Santonian, as described and illustrated by Moustafa (2008) and Bosworth et al. (2008). Nevertheless, any reverse reactivation of faults within the eastern Abu Gharadig Basin study area within this time interval was minor, such that faults retain net extensional offsets. Structural shortening thus appears to have been focused onto faults of appropriate strike on the main northern basin margin (the Mubarak Inversion trend of Bosworth et al., 2008).

The near the top of Khoman B to near the top of Khoman A interval in the Abu Gharadig Basin study area shows further thickness differentials associated with the central saddle, implying extensional faulting continued into this stratigraphic phase. However, across the basin more dramatic unconformities are clear at the top of the Khoman B Member and within the Khoman A Member (Figure 10, after Moustafa, 2008), and these converge toward the northern basin margin (Moustafa, 2008; Bosworth et al., 2008). It is therefore difficult to be precise with respect to when preferential subsidence and sediment accumulation to the north-west and southeast of the central saddle switched from being due to normal faulting to due to inversion of basin margin structures. Compressive strain was localised onto the northern basin margin (see Figure 2D of Bosworth et al., 2008), but extension may have continued on structures of suitable orientation, such as the NW-SE trending basin margin fault (F1 in Figure 4b). It is not clear whether the central saddle antiform underwent any tightening associated with these inversion events, but net normal offsets remain on all the intrabasinal faults in the study area.

Above the Maastrichtian-Palaeogene unconformity, the interval from near the top of Khoman A to near the top of Dabaa Formation thickens to the NNW, consistent with extensional reactivation of the northern basin-bounding fault set and to the northeast, on the downthrown side of the F1 basin-bounding fault. There is no sign of thickening southeastwards. E-W to WNW-ESE oriented intrabasinal faults show normal fault reactivation (Figure 6d). So a pulse of rifting involving tilting down to the north can be invoked. The lack of expression of the central saddle suggests that any normal fault-related growth or inversion-related tightening of this structure had ceased by Apollonia Formation times. This however, does not preclude further inversion on the northern basin margin continuing after burial of the base-Palaeogene unconformity in the eastern Abu Gharadig Basin.

This study highlights the value of mapping at a high stratigraphic resolution to identify subtle changes in the local stress regime of sedimentary basins, which have undergone pulses of rifting and inversion. Basins across the West and Central African rift system and the rifts of North-East Africa were deforming in response to Late Cretaceous rifting, collision-related inversion, and regional dextral shear (Fairhead et al., 2013). In such shear-influenced settings, the Gindi Basin provides an example of how certain basins may show short-lived inversion or “pop-up” events in response to local changes in principal stress directions or their relative magnitudes. However, these events may only be characterized when isochron and isochore mapping is carried out at the scale of age (e.g. Turonian) or shorter time intervals. The recognition of a Mid- to Upper Turonian inversion event in the Gindi Basin suggests that other subtle pop-up phases on structures of suitable orientation might have occurred and should be searched for in other West, Central and Northeast African rift basins earlier than the main Santonian-Palaeogene inversions described.

In conclusion, how Late Cretaceous tectonic inversion processes affected the northern Western Desert varies from one sedimentary basin to another. The Abu Gharadig Basin and the Gindi Basin are two examples, which display different styles and timing of inversion events. The inversion in the Abu Gharadig Basin was focused on its northern basin margin. In contrast, in the Gindi Basin, the NE-SW striking, intrabasinal rift faults allow a Mid- to Upper Turonian inversion to be identified.

Acknowledgements

The authors are grateful to the Khalda Petroleum Company and the Qarun Petroleum Company in Egypt for providing the data presented in this article and to the Egyptian General Petroleum Corporation (EGPC) for permission to present these data. Dr. M. Sarhan acknowledges the Egyptian Government for Post-Doctorate Academic Visiting Scheme funding of a stay at the University of Leeds and the University of Leeds for hosting and for access to facilities. Thanks to Ahmad Said and Reda Abdel Ghany, Qarun Petroleum Company for their help and fruitful discussions. Many thanks for anonymous referees for their constructive comments on the manuscript. We are so grateful to Prof. Dr. Read Mapeo, the Editor-in-Chief of the Journal of African Earth sciences for his efforts and time in critically reviewing the manuscript and for his valuable comments.

References

Abdel-Kireem, M. R., and Ibrahim, M. I. A. (1987). Late Cretaceous biostratigraphy and palaeobathymetry of the Betty Well No. 1, Western Desert, Egypt. In: Colloquium on African Geology, 14, pp. 165-169.

Abdel-Kireem, M. R., Schrank, E., Samir, A. M., and Ibrahim, M. I. A. (1996). Cretaceous palaeoecology, palaeogeography and palaeoclimatology of the northern Western Desert, Egypt. Journal of African Earth Sciences, 22(1), 93-112.

Bakry, G. (1993). Contribution to the geology and hydrocarbon potential of the Mesozoic rocks in the area between Quarun and Cairo-Suez district. Unpublished Dissertation Thesis, Geology Department, Al Azhar University, Cairo. 176 pp.

Bally, A. W. (1983). Seismic expression of structural styles. AAPG Studies in geology, 15(3).

Bally, A.W., (1984). Tectogenèse et sismique réflexion. Bulletin de la Societe Geologique de France 26, 279–285.

Bayoumi, A. I., and Lotfy, H. I. (1989). Modes of structural evolution of Abu Gharadig Basin, Western Desert of Egypt as deduced from seismic data. Journal of African Earth Sciences (and the Middle East), 9(2), 273-287.

Bonini, M., Sani, F., and Antonielli, B. (2012). Basin inversion and contractional reactivation of inherited normal faults: A review based on previous and new experimental models. Tectonophysics, 522, 55-88.

Bosworth, W. (1994). A model for the three-dimensional evolution of continental rift basins, north-east Africa. Geologische Rundschau, 83(4), 671-688.

Bosworth, W., El-Hawat, A. S., Helgeson, D. E., and Burke, K. (2008). Cyrenaican "shock absorber" and associated inversion strain shadow in the collision zone of northeast Africa. Geology, 36(9), 695-698.

Cartwright, J.A., Trudgill, B.D. and Mansfield, C.S., (1995). Fault growth by segment linkage: an explanation for scatter in maximum displacement and trace length data from the Canyonlands Grabens of SE Utah. Journal of Structural Geology, 17(9), 1319-1326.

Cathro, D. L., and Karner, G. D. (2006). Cretaceous–Tertiary inversion history of the Dampier Sub-basin, northwest Australia: insights from quantitative basin modelling. Marine and Petroleum Geology, 23(4), 503-526.

Contreras, J., Anders, M.H. and Scholz, C.H. (2000). Growth of a normal fault system; observations from the Lake Malawi basin of the East African Rift. Journal of Structural Geology, 22, 159-168.

Cooper, M.A., Williams, G.D. (Eds.), (1989). Inversion Tectonics, 44. Geological Society of London Special Publication. 375 pp.

Coward, M.P., Gillcrist, R., Trudgill, B., (1991). Extensional structures and their tectonic inversion in the Western Alps. In: Roberts, A.M., Yielding, G., Freeman, B. (Eds.), The Geometry of Normal Faults, 56. Geological Society Special Publication, pp. 93–113.

David M. Allard1, David W. Phelps1, John R. Bedingfield1, Gregg S. Barker1 (1) Apache Egypt Companies, Houston, TX (2003). Egyptian Western Desert Jurassic and Cretaceous Structural Styles, AAPG International Conference, Barcelona, Spain.

Dawers, N.H., Underhill, J.R. 2000. The role of fault interaction and linkage in controlling synrift stratigraphic sequences: Stratfjord East area, Northern North Sea. AAPG Bulletin, 84;1, 45-64.

EGPC (Egyptian General Petroleum Corporation), (1992). Western Desert, oil and Gas fields, A comprehensive overview. 11 EGPC Expl. and Prod. Conf. Cairo., pp: 1-431.

Ellis, P. G., and McClay, K. R. (1988). Listric extensional fault systems-results of analogue model experiments. Basin Research, 1(1), 55-70.

Fairhead, J. D., Green, C. M., Masterton, S. M., and Guiraud, R. (2013). The role that plate tectonics, inferred stress changes and stratigraphic unconformities have on the evolution of the West and Central African Rift System and the Atlantic continental margins. Tectonophysics, 594, 118-127.

Fawzy, A., and Dahi, M. (1992). Regional geological evaluation of the Western Desert, Egypt. Geology of the Arab World, 1, 111-149.

Fraser, A. J. and Gawthorpe, R. L. (1990). Tectonostratigraphic development and hydrocarbon habitat of the Carboniferous in northern England. In: Hardman, R. F. P. and Brooks, J. (eds) Tectonic Events Responsible for Britain's Oil and Gas Reserves. Geological Society, London, Special Publication, 55, 49-86.

Frizon de Lemotte, D., Raulin, C., Mouchot, N., Wrobel-Daveau, J.-C., Blanpied, C. and Ringenbach, J.-C. (2011). The southernmost margin of the Tethys realm during the Mesozoic and Cenozoic: Initial geometry and timing of the inversion process. Tectonics, 30, TC3002, doi:101029/2010TC002691.

Guiraud, R. (1998). Mesozoic rifting and basin inversion along the northern African Tethyan margin: an overview. Geological Society, London, Special Publications, 132(1), 217-229.

Hantar, G. (1990). North Western Desert. Geology of Egypt, 293-327.

Mahsoub, M., Abulnasr, R., Boukhary, M., Faris, M., and Abd El Aal, M. (2012). Bio-and Sequence Stratigraphy of Upper Cretaceous–Palaeogene rocks, East Bahariya Concession, Western Desert, Egypt. Geologia Croatica, 65(2), 109-138.

Morley, C. K., Nelson, R. A., Patton, T. L., and Munn, S. G. (1990). Transfer zones in the East African rift system and their relevance to hydrocarbon exploration in rifts (1). AAPG Bulletin, 74(8), 1234-1253.

Moustafa, A. R. (2013). Fold-related faults in the Syrian Arc belt of northern Egypt. Marine and Petroleum Geology, 48, 441-454.

Moustafa, A.R., 2008. Mesozoic-Cainozoic basin evolution in the northern Western Desert of Egypt. In: Salem, M., El-Arnauti, A., Saleh, A. (Eds.), 3rd Symposium on the Sedimentary Basins of Libya, The Geology of East Libya, vol. 3, pp. 29-46.

Nogueira, F. C., Marques, F. O., Bezerra, F. H., de Castro, D. L., and Fuck, R. A. (2015). Cretaceous intracontinental rifting and post-rift inversion in NE Brazil: Insights from the Rio do Peixe Basin. Tectonophysics 644–645 (2015) 92–107.

Paton, D.A. and Underhill, J.R. (2004). Role of crustal anisotropy in modifying the structural and sedimentological evolution of extensional basins: the Gamtoos Basin, South Africa. Basin Research, 16, 339-359.

Rotevatn, A and Jackson, C.A.-L. (2014). 3D structure and evolution of folds during normal fault dip linkage. Journal of the Geological Society, 171 (6), 821-829.

Salè, S. O., Guimerà, J., Mas, R., and Arribas, J. (2014). Tectono-stratigraphic evolution of an inverted extensional basin: the Cameros Basin (north of Spain). International Journal of Earth Sciences, 103(6), 1597-1620.

Sarhan, M. A. (2017a). Seismic–Wireline logs sequence stratigraphic analyses and geologic evolution for the Upper Cretaceous succession of Abu Gharadig basin, Egypt. Journal of African Earth Sciences, 129, 469-480.

Sarhan, M. A. (2017b). Wrench tectonics of Abu Gharadig Basin, Western Desert, Egypt: a structural analysis for hydrocarbon prospects. Arabian Journal of Geosciences,10(18), 399.

Sarhan, M. A., Basal, A. M. K. and Ibrahim, I. M. (2017a). Seismic and well logging interpretation for evaluation of the lower Bahariya reservoir, southwest Qarun (SWQ) Field, Gindi Basin, Egypt. Marine Geophysical Research, 38(3), 271-290.

Sarhan, M. A., Basal, A. M. K., and Ibrahim, I. M. (2017b). Integration of seismic interpretation and well logging analysis of Abu Roash D Member, Gindi Basin, Egypt: Implication for detecting and evaluating fractured carbonate reservoirs. Journal of African Earth Sciences, 135, 1-13.

Schlische, R. W. (1995). Geometry and origin of fault-related folds in extensional settings. AAPG bulletin, 79(11), 1661-1678.

Schlumberger (1984). Well evaluation conference, Egypt. Schlumberger Middle East S.A., pp. 1–64.

Schrank, E., and Ibrahim, M. I. (1995). Cretaceous (Aptian-Maastrichtian) palynology of foraminifera-dated wells (KRM-1, AG-18) in northwestern Egypt. Selbstverlag Fachbereich Geowissenschaften, vol. 177, FU Berlin.

Scisciani, V., (2009). Styles of positive inversion tectonics in the Central Apennines and in the Adriatic foreland: implications for the evolution of the Apennine chain (Italy). Journal of Structural Geology 31, 1276–1294.

Sibson, R. H. (1995). Selective fault reactivation during basin inversion: potential for fluid redistribution through fault-valve action. Geological Society, London, Special Publications, 88(1), 3-19.

Soliman, S. M., and El Badry, O. (1970). Nature of Cretaceous sedimentation in Western Desert, Egypt. AAPG Bulletin, 54(12), 2349-2370.

Sultan, N., and Abd El Halim, M. (1988). Tectonic framework of northern Western Desert, Egypt and its effect on hydrocarbon accumulations. Proc. 9th Exploration and Production Conference, Egyptian General Petroleum Corporation, Cairo, 2, 1-22.

Tantawy, A. A., Keller, G., Adatte, T., Stinnesbeck, W., Kassab, A., and Schulte, P. (2001). Maastrichtian to Palaeocene depositional environment of the Dakhla Formation, Western Desert, Egypt: sedimentology, mineralogy, and integrated micro-and macrofossil biostratigraphies. Cretaceous Research, 22(6), 795-827.

Tavarnelli, E., (1996). Tethyan heritage in the development of the Neogene Umbria– Marche fold-and-thrust belt, Italy: a 3D approach. Terra Nova 8, 470–478.

Turner, J.P., Williams, G.A., (2004). Sedimentary basin inversion and intra-plate shortening. Earth-Science Reviews 65, 277–304.

Wescott,W. A., Atta, M., Blanchard, D.C., Cole, R. M., Georgeson, S. T., Miller, D. A., O'Hayer, W. W., Wilson, A. D., Dolson, J. C., Sehim, A. (2011). Jurassic Rift Architecture in the Northeastern Western Desert, Egypt. Search and Discovery Article #10379 Posted December 19, 2011 *Adapted from poster presentation at AAPG International Conference and Exhibition, Milan, Italy, October 23-26, 2011.

Wilson, P., Gawthorpe, R. L., Hodgetts, D., Rarity, F., and Sharp, I. R. (2009). Geometry and architecture of faults in a syn-rift normal fault array: the Nukhul half-graben, Suez rift, Egypt. Journal of Structural Geology, 31(8), 759-775.

Withjack, M.O., Baum, M.S., Schlische, R.W., (2010). Influence of preexisting fault fabric on inversion-related deformation: a case study of the inverted Fundy rift basin, southeastern Canada. Tectonics 29. doi:10.1029/2010TC002744 TC6004.

Ziegler, P. A. (1987). Late Cretaceous and Cenozoic intra-plate compressional deformations in the Alpine foreland—a geodynamic model. Tectonophysics, 137(1), 389-420.

Figures Captions

Fig. (1) Regional map highlighting the study areas within the Abu Gharadig Basin and the Gindi Basin in the northern Western Desert (after Bosworth et al, 2008). See Figure 3 for data distributions in the boxed study areas.

.

Fig. (2) Regional stratigraphic column of the northern part of the Egyptian Western Desert including the Abu Gharadig and Gindi Basins (stratigraphic nomenclature after Moustafa, 2008). Lithostratigraphic column is based on the well data used in this study.

Fig. (3) Available seismic lines and well locations of the study areas. (A) Abu Gharadig Basin and (B) Gindi Basin.

Fig. (4) Interpreted seismic lines within the Abu Gharadig Basin. (A) Dip seismic line no. 1390 and (B) strike line no. 5240 (see Fig. 3 for relative locations), which shows long-lived growth into fault F1, coloured red, and an oblique section through the central Abu Gharadig anticline prominent at Top Abu Roash D level (pale blue).

Fig. (5) Time-depth contour maps (ms TWT) of the picked seismic horizons within the Abu Gharadig Basin. (A) Top Bahariya Formation, (B) Top Abu Roash D Member, (C) Near the top of Khoman B Member, (D) Near the top of Khoman A Member, (E) Near the top of Dabaa Formation. Note the NE-SW trending, NE-plunging central anticline in (A) and (B).

Fig. (6) Time-thickness contour maps (ms TWT) of the picked seismic intervals within the Abu Gharadig Basin. (A) From Top Bahariya Formation to Top Abu Roash D Member, (B) from Top Abu Roash D Member to near the top of Khoman B Member, (C) from near the top of Khoman B Member to near the top of Khoman A Member, (D) from near the top of Khoman A Member to near the top of Dabaa Formation. Note the thickening to the NW and to the ESE of the central NE-SW trending anticline or saddle, most prominent during the (B) Top Abu Roash D to near the top of Khoman B interval.

Fig. (7) Interpreted seismic lines within the Gindi Basin, showing its central anticline. (A) Dip line no. 4766 and (B) strike line no. 10476 (see Fig. 3 for relative locations).

Fig. (8) Time-depth contour maps (ms TWT) of the picked seismic horizons within the Gindi Basin, characterizing the prominent NE-SW anticline. (A) Top Bahariya Formation, (B) Top Abu Roash F Member, (C) Top Abu Roash D Member, (D) Top Abu Roash B Member.

Fig. (9) Time-thickness contour maps (ms TWT) of the picked seismic intervals within the Gindi Basin. (A) From Top Bahariya Formation to Top Abu Roash F Member, (B) from Top Abu Roash F Member to Top Abu Roash D Member, (C) from Top Abu Roash D Member to Top Abu Roash B Member. Note the switch from minor graben development (interval A) to thinning onto the crest of the structure and inferred inversion during intervals B and C.

Fig. (10) Sketch modified from an interpreted E-W seismic profile in Moustafa (2008) across the Abu Gharadig Basin showing the positive structural inversion of a NE-SW oriented basin margin fault during the Santonian to Palaeogene. Orange arrows denote directions of reflector (strata) terminations.

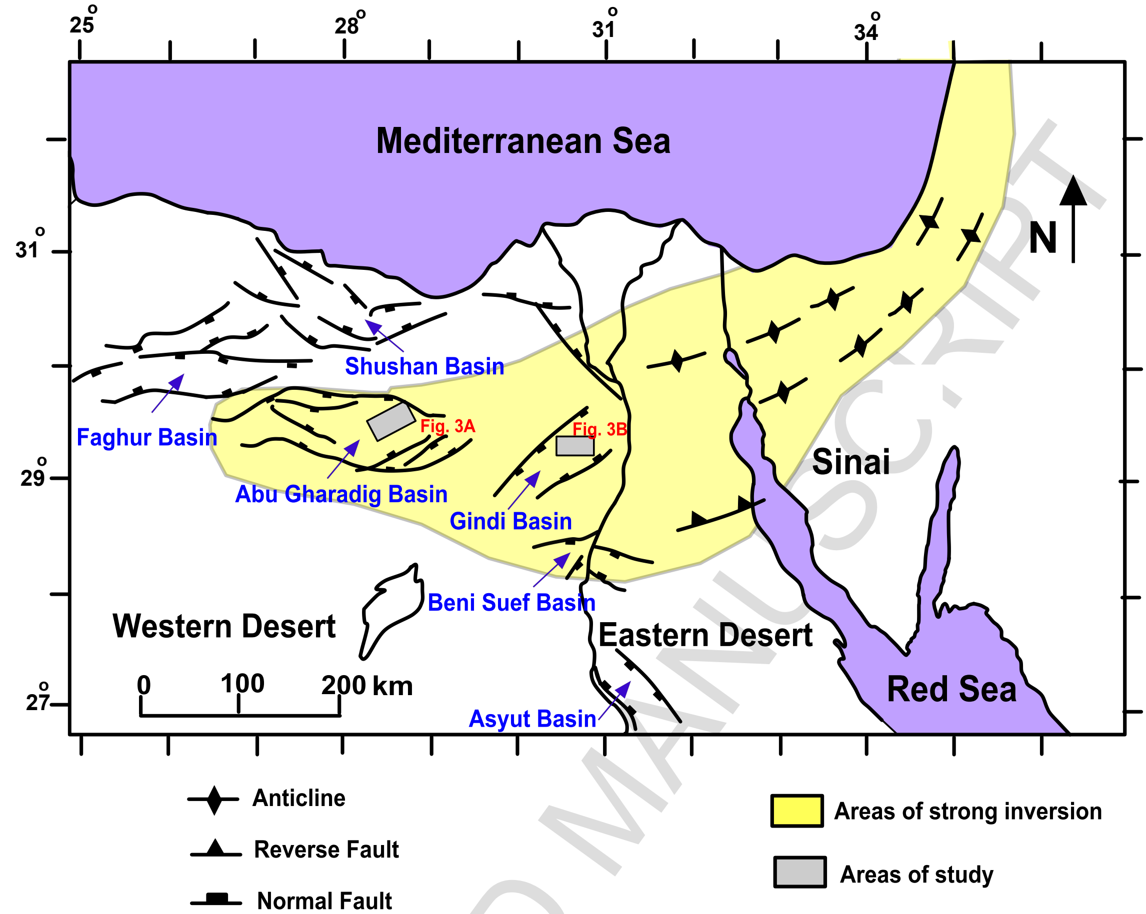
25°
28°
31°
34°
31°
29°
27°
Mediterranean Sea
N
Shushan Basin
Faghur Basin
Fig. 3A
Fig. 3B
Abu Gharadig Basin
Gindi Basin
Sinai
Beni Suef Basin
Western Desert
Eastern Desert
0
100
200 km
Red Sea
Asyut Basin
Anticline
Reverse Fault
Normal Fault
Areas of strong inversion
Areas of study

Figure 1

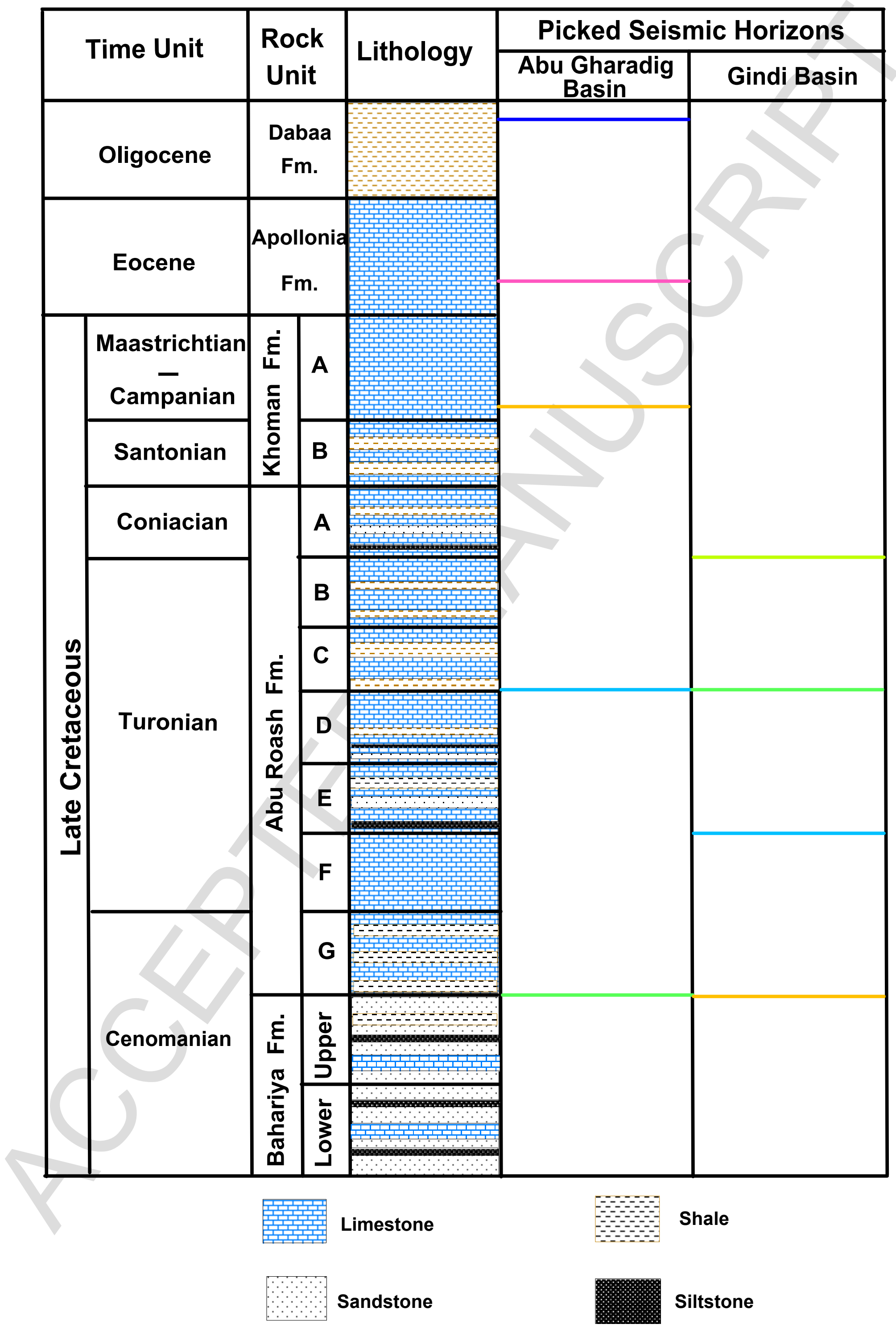
Time Unit
Rock Unit
Lithology
Picked Seismic Horizons
Abu Gharadig Basin
Gindi Basin
Oligocene
Dabaa Fm.
Eocene
Apollonia Fm.
Late Cretaceous
Maastrichtian – Campanian
Santonian
Coniacian
Turonian
Cenomanian
Khoman Fm.
A
B
Abu Roash Fm.
A
B
C
D
E
F
G
Bahariya Fm.
Upper
Lower
Limestone
Shale
Sandstone
Siltstone

Figure 2

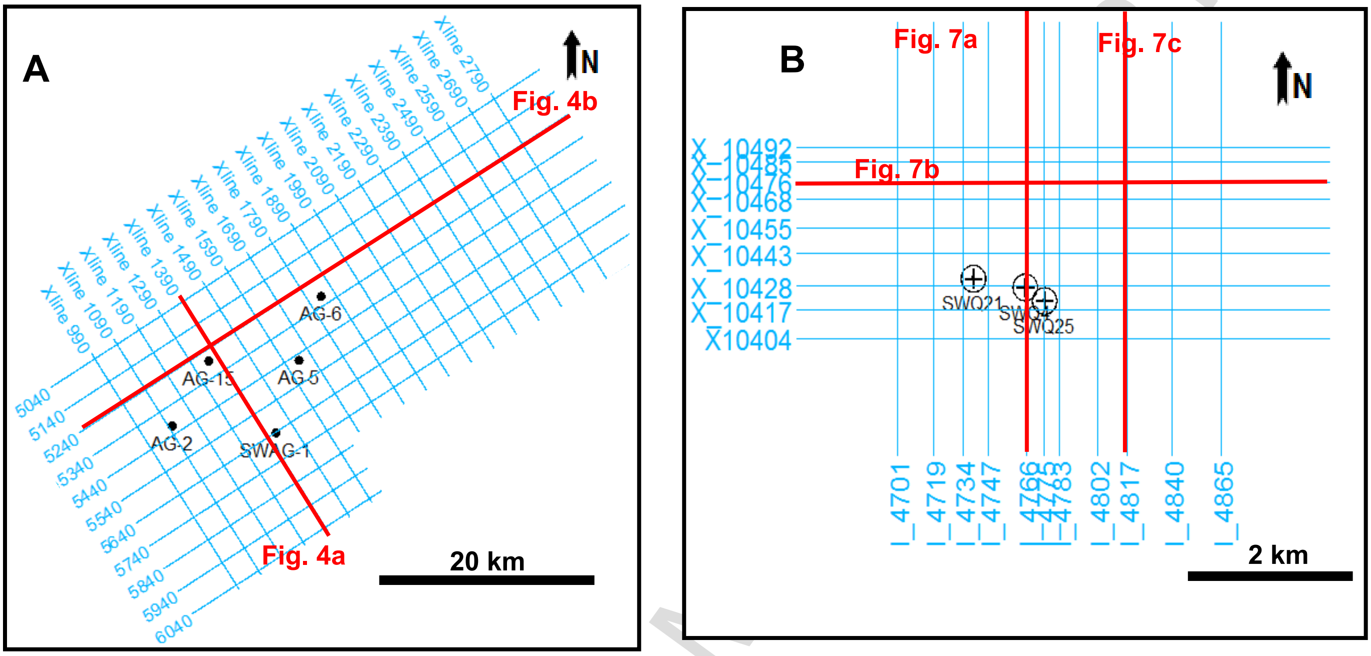
A
B
N
Fig. 4a
Fig. 4b
20 km
AG-6
AG-15
AG-5
AG-2
SWAG-1
Fig. 7a
Fig. 7b
Fig. 7c
2 km
SWQ21
SWQ25

Figure 3

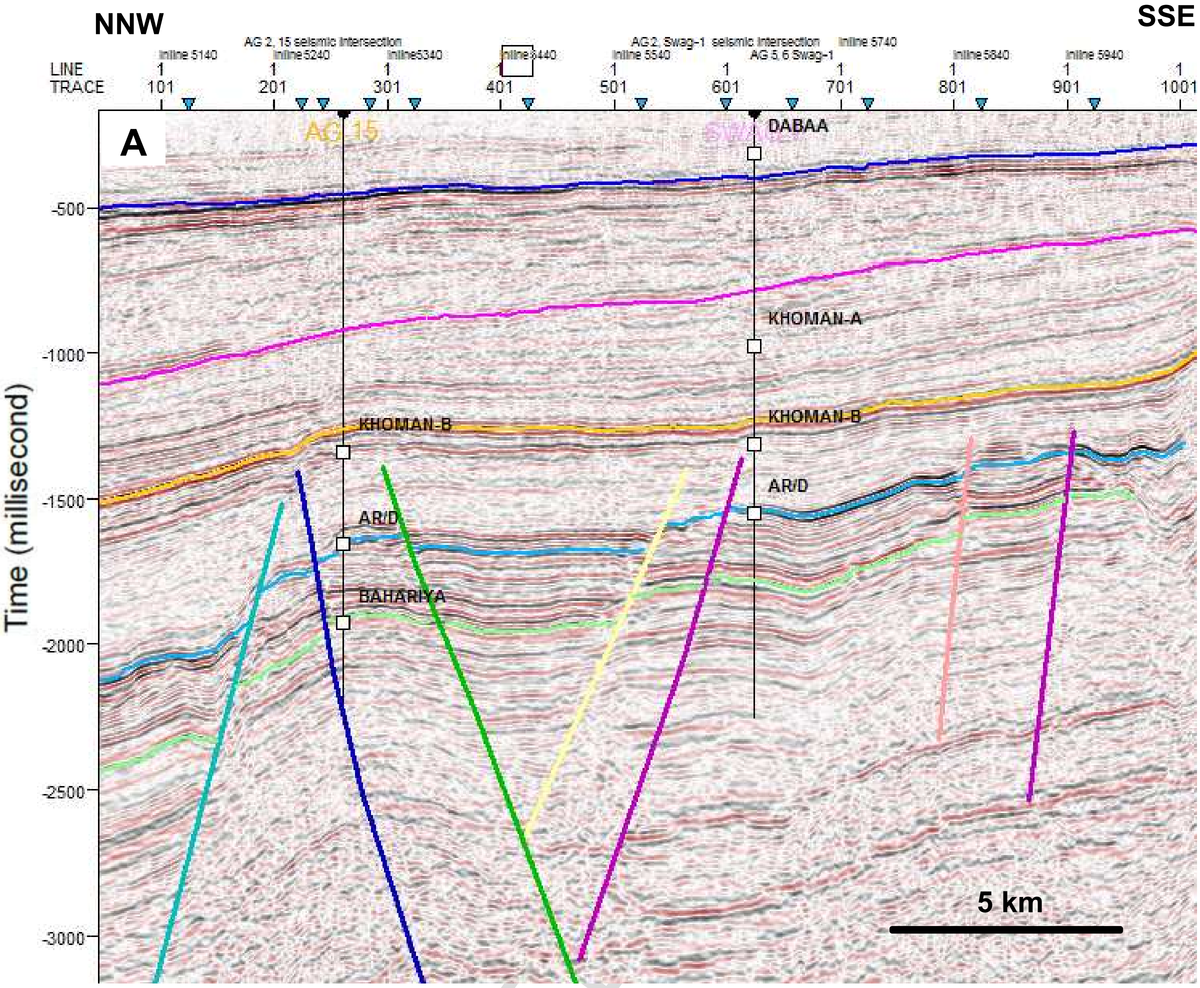

NNW
SSE
A
AG 2, 15 seismic intersection
AG 2, Swag-1 seismic intersection
AG 5, 6 Swag-1
LINE
TRACE
AG 15
DABAA
KHOMAN-A
KHOMAN-B
AR/D
BAHARIYA
Time (millisecond)
-500
-1000
-1500
-2000
-2500
-3000
5 km

Figure 4a

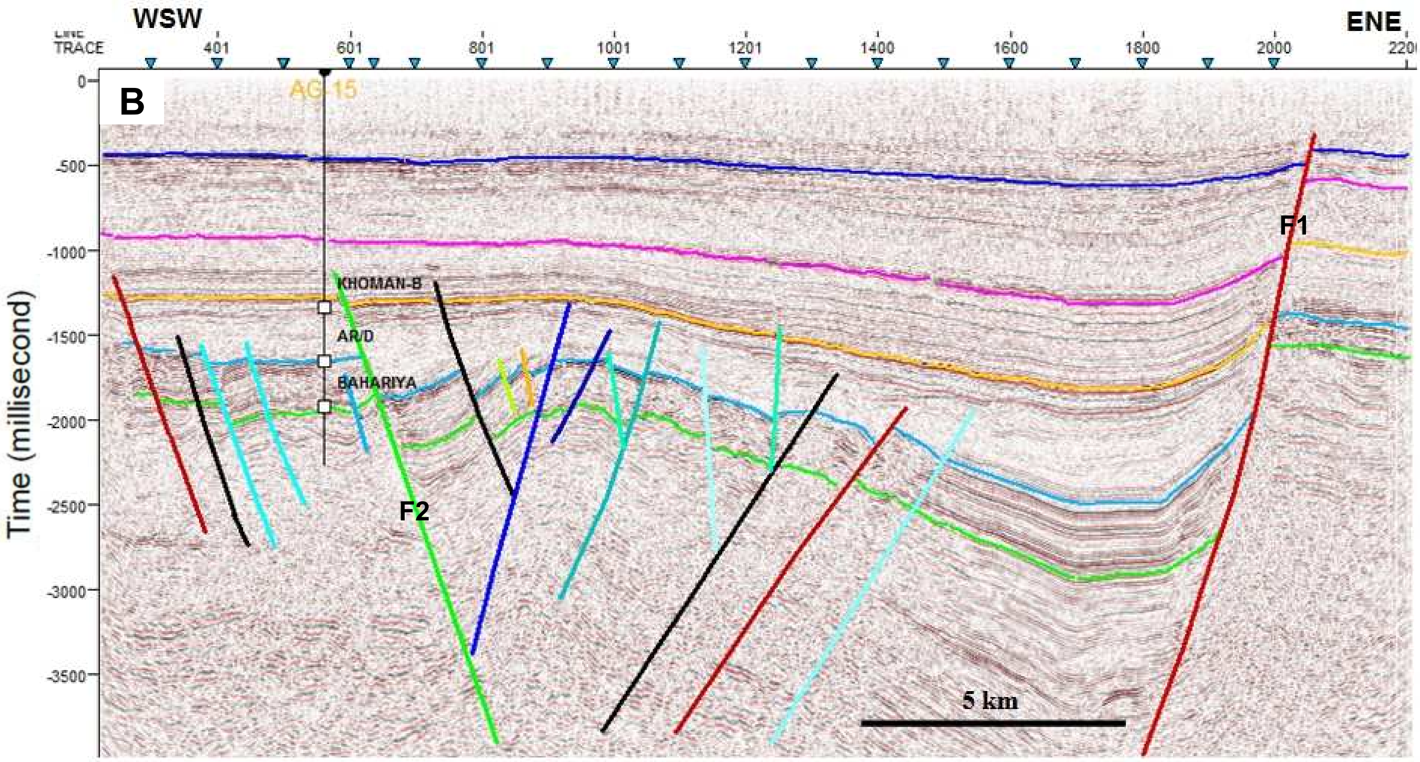

WSW
ENE
LINE TRACE
401
601
801
1001
1201
1400
1600
1800
2000
B
AG-15
KHOMAN-B
AR/D
BAHARIYA
F1
F2
Time (millisecond)
0
-500
-1000
-1500
-2000
-2500
-3000
-3500
5 km

Figure 4b

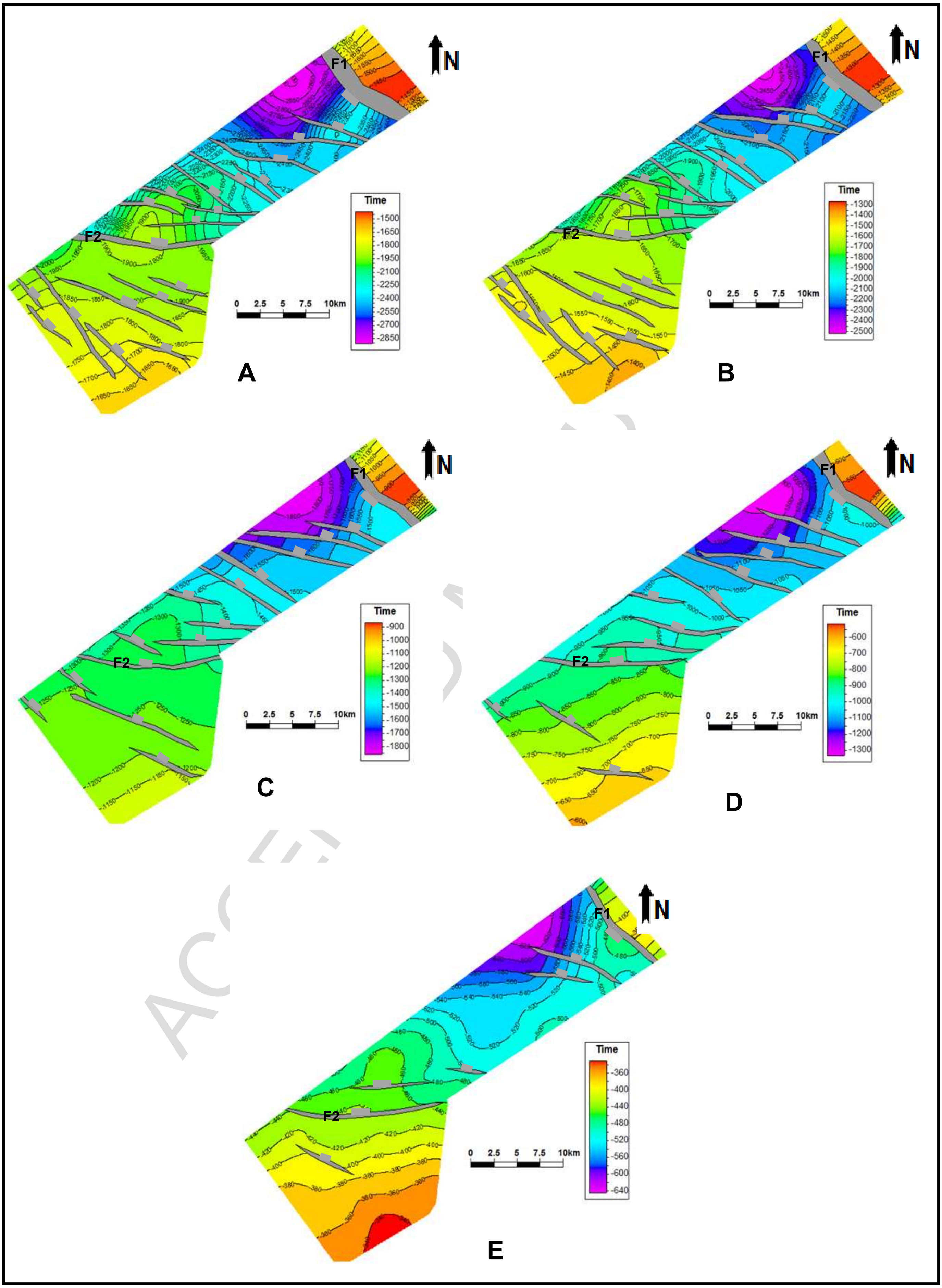

Figure 5

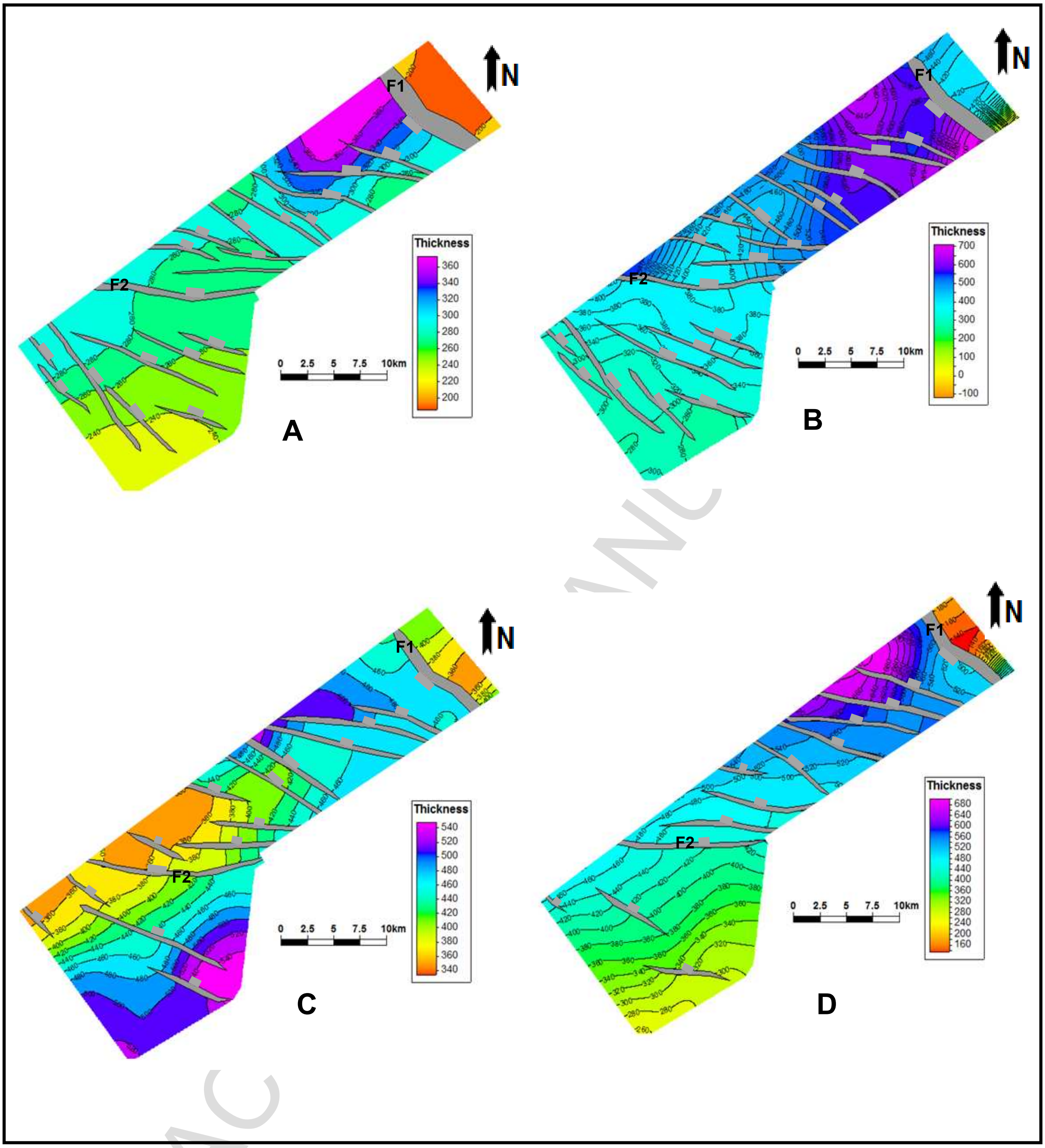

Figure 6

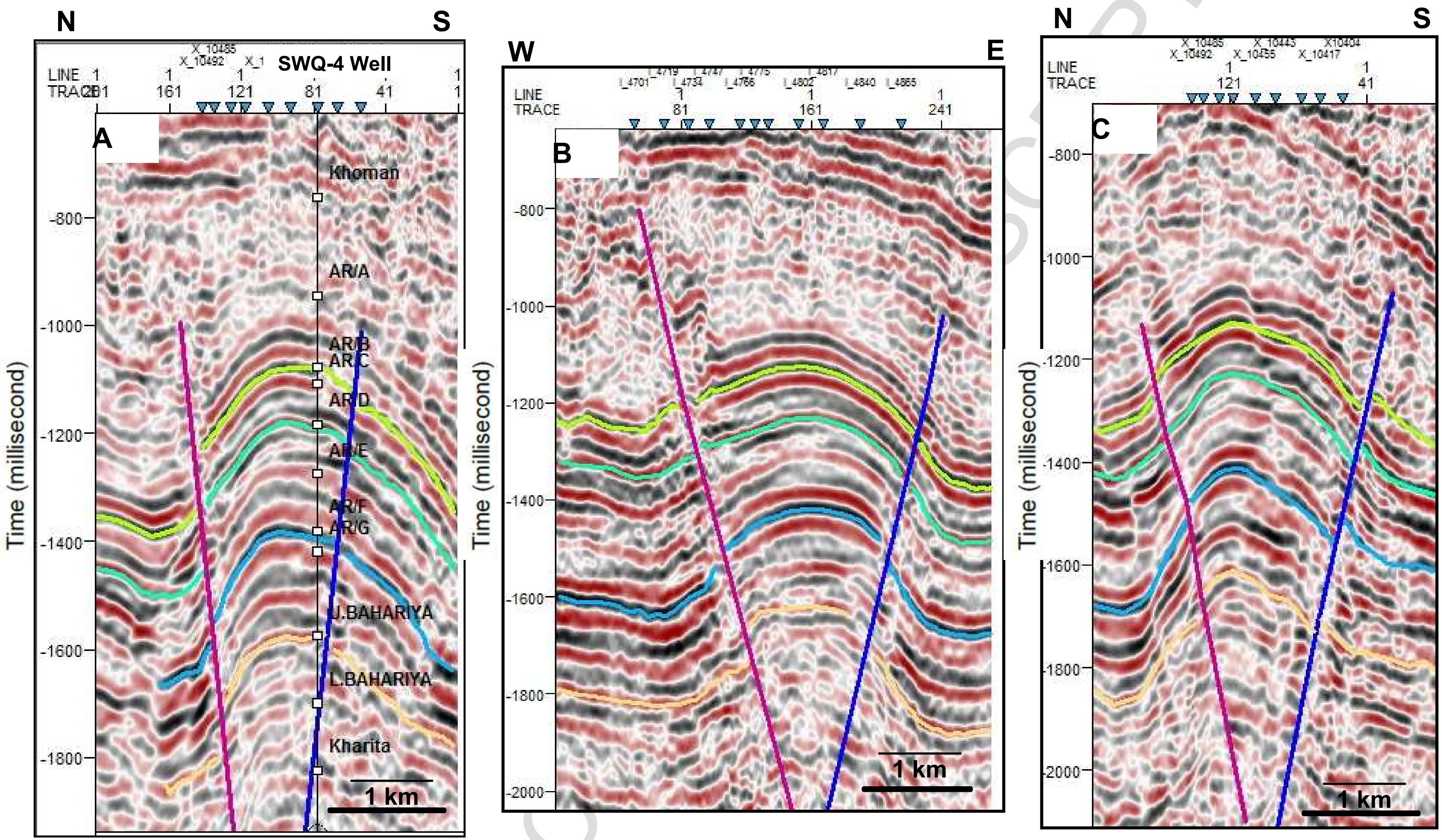
N
S
SWQ-4 Well
LINE
TRACE
A
Khoman
AR/A
AR/B
AR/C
AR/D
AR/E
AR/F
AR/G
U.BAHARIYA
L.BAHARIYA
Kharita
1 km
Time (millisecond)
W
E
B
1 km
Time (millisecond)
N
S
C
1 km
Time (millisecond)

Figure 7

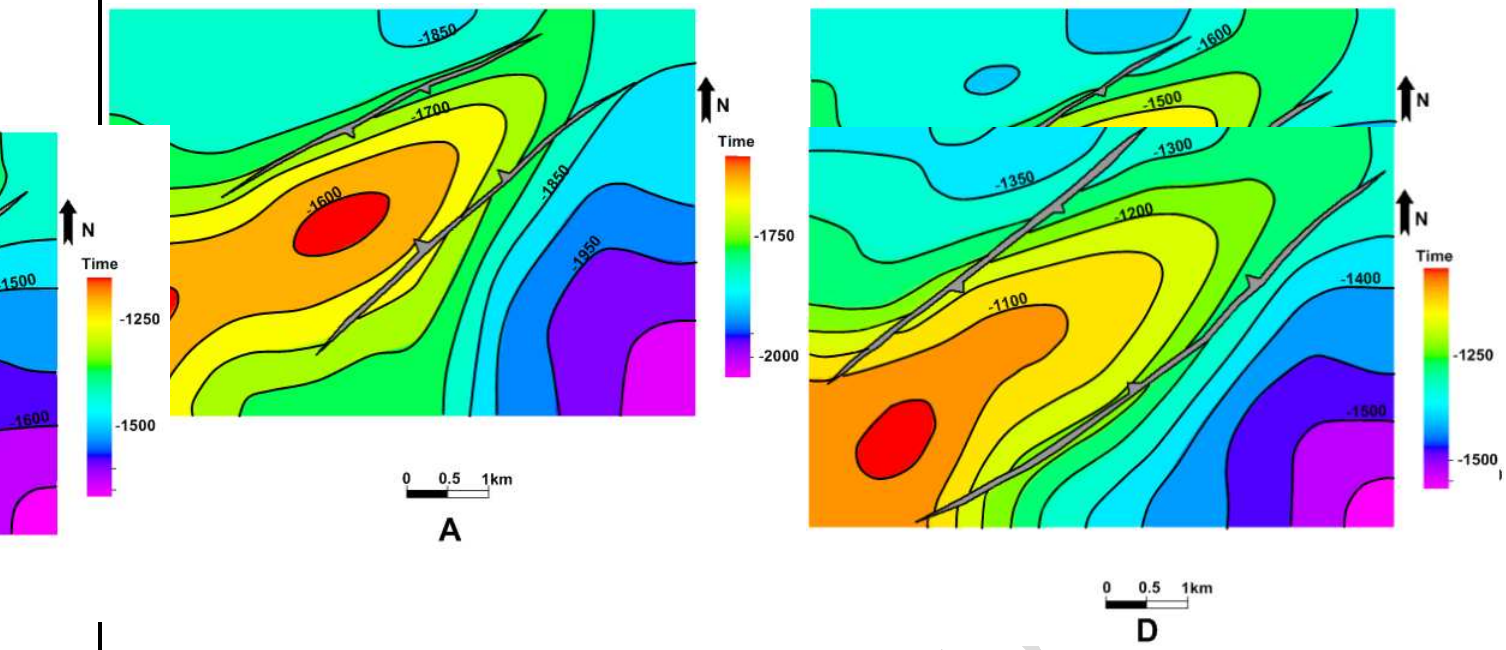

-1850
-1700
-1600
-1850
-1950
N
Time
-1750
-2000
-1500
-1250
-1500
-1600
0 0.5 1km
A
-1600
-1500
-1300
-1350
-1200
-1100
-1400
-1500
-1250
-1500
0 0.5 1km
D

Figure 8

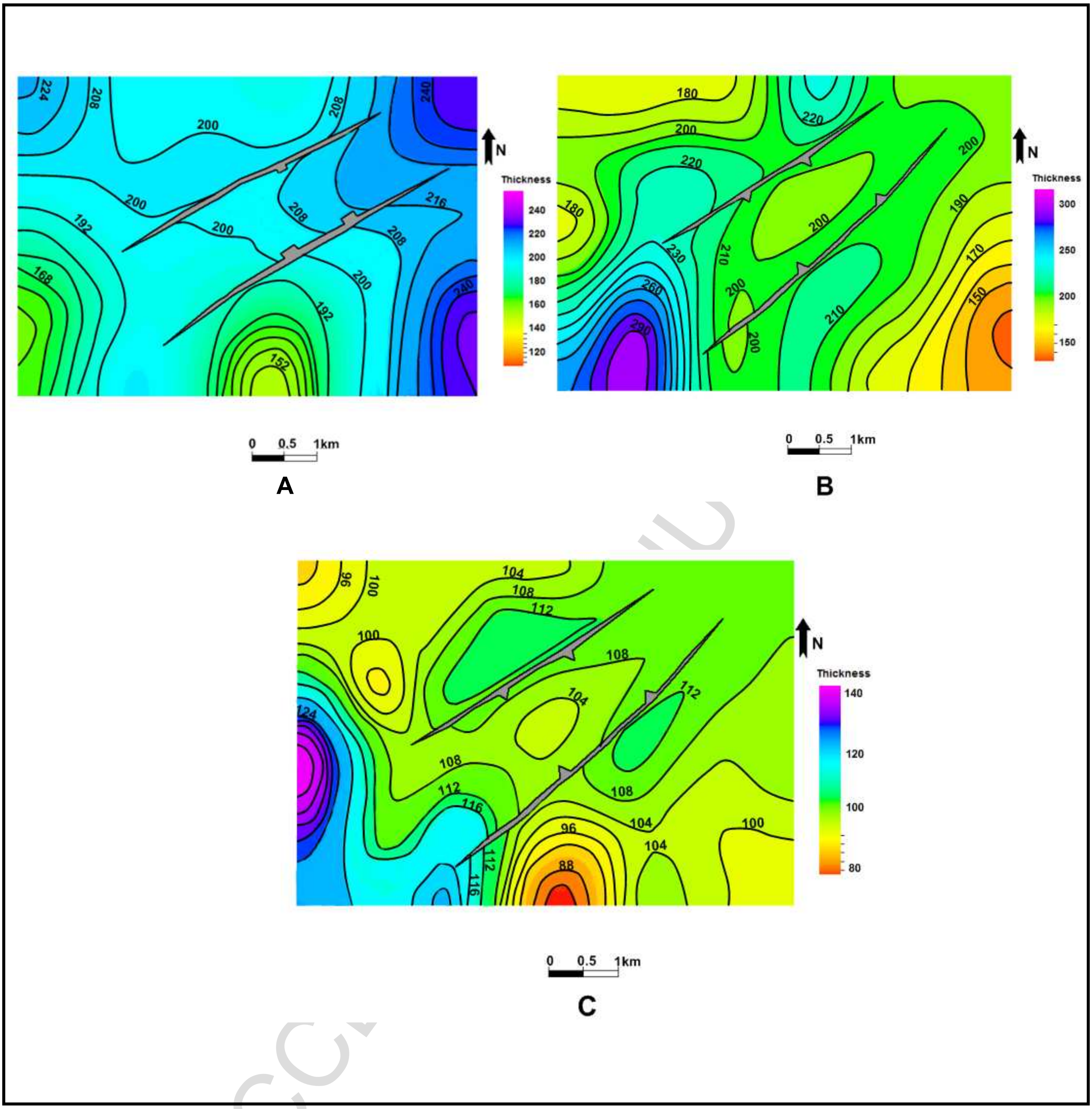

Figure 9

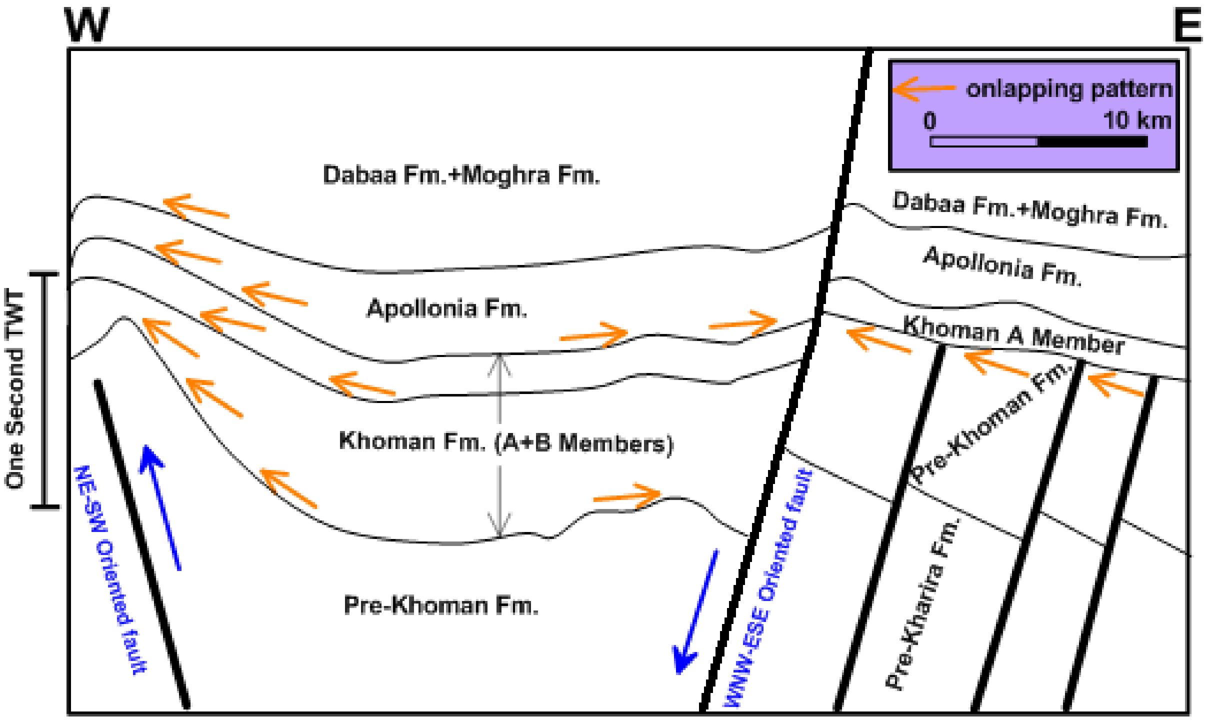
W
E
onlapping pattern
0
10 km
Dabaa Fm.+Moghra Fm.
Apollonia Fm.
Khoman Fm. (A+B Members)
Pre-Khoman Fm.
Dabaa Fm.+Moghra Fm.
Apollonia Fm.
Khoman A Member
Pre-Khoman Fm.
Pre-Kharira Fm.
One Second TWT
NE-SW Oriented fault
WNW-ESE Oriented fault

Figure 10

Highlights

1- Rift-related and inversion-related anticlines.

2- Tectonic inversion in the Abu Gharadig and Gindi Basins.

3- Value of mapping at high stratigraphic resolution.